An Observer Study Evaluating Dual-Plane Circular-Orbit Cone-Beam Brain SPECT

David S. Lalush, PhD, and Andrew J. DiMeo, MS

Department of Biomedical Engineering, University of North Carolina at Chapel Hill, Chapel Hill, North Carolina

Dual-plane circular-orbit cone-beam (DPCB) SPECT uses a pair of dissimilar cone-beam collimators to expand the axial field of view for brain SPECT. We applied observer study methodology to evaluate the improvement in detection of small defects in brain perfusion provided by DPCB SPECT, compared with conventional parallel-beam imaging. We also evaluated the effect of changing the radius of rotation on DPCB imaging. **Methods:** Images were realistically simulated using a brain phantom. High-count Monte Carlo simulations were performed for 4 imaging configurations: low-energy high-resolution parallel-beam imaging at a radius of rotation of 18 cm and DPCB imaging (52-cm focal length) at radii of rotation of 20, 24, and 28 cm. These distances corresponded to those required for our camera to clear the shoulders of a patient in the 5th, 50th, and 95th percentiles of shoulder width. Perfusion defects of ~1.8-cm diameter were simulated at 4 locations in the brain. Poisson noise was simulated, and images were reconstructed to create a set of 200 images for each of the 4 configurations. All reconstructions used ordered-subset expectation maximization with attenuation modeling. Eight observers viewed images on which the possible location of the defect was marked. The observers were trained using 384 images, were tested using 416 images, and rated on a continuous scale their confidence about the presence of a defect. **Results:** Using a paired *t* test for the estimated areas under the receiver operating characteristic (ROC) curve for each observer, we found that all 3 DPCB configurations resulted in higher areas under the ROC curve than did the parallel-beam configuration. Further, area under the ROC curve for the DPCB configurations improved with decreasing radius of rotation. All comparisons were significant at $P < 0.05$, except for DPCB 20 cm to DPCB 24 cm ($P = 0.089$). **Conclusion:** Use of a dual-plane cone beam is feasible for brain SPECT and better detects small perfusion defects than does a parallel beam, despite the possibility that the radius of rotation will need to be increased significantly to clear the patient's shoulders. A dual-plane cone beam should be used with the shortest radius of rotation possible to maximize the detectability of small perfusion defects.

Key Words: brain SPECT; cone-beam SPECT

J Nucl Med 2002; 43:1578–1583

Converging-beam collimators for SPECT can improve both spatial resolution and detection efficiency (*1–3*). The principal cost of using such collimators, compared with parallel-beam imaging, is the reduction in field of view. Decreasing the focal length of such collimators further magnifies the advantages and problems: The resolution-efficiency tradeoff improves, but field of view decreases. Because of the limitations on field of view, cone-beam collimation has generally been usable only for applications requiring a relatively small field of view in both transverse and axial directions (*1,3*). Several factors, however, limit the minimum focal length that can be achieved in brain imaging: principally, the field of view required to view the entire head, and the need for the rotating gantry to clear the patient's shoulders.

Several potential solutions have been proposed for brain SPECT. These include a tilted-camera cone beam (*2*) and the use of cone-beam collimators with focal points drastically offset in the axial direction (*4*). Both methods seek to get the camera as close to the subject's head as possible while avoiding the shoulders entirely.

Dual-plane circular-orbit cone-beam (DPCB) SPECT (*5,6*) was developed to address these problems on conventional dual-camera scanners capable of only planar rotations of the gantry. The DPCB method, illustrated in Figure 1, uses 2 dissimilar collimators with focal points offset in the axial direction. This design effectively permits a shorter focal length for the same axial field of view as is obtained with a conventional cone-beam collimator, assuming that the axial field of view is defined as the region viewed by at least 1 camera. Although 1 camera may not view a region near the top or bottom of the brain, the other camera will, so that truncation artifacts are avoided. Noise statistics will, however, be different in regions viewed by only a single camera.

Because the DPCB design requires that the camera rotate clear of the shoulders, larger radii of rotation will be required for DPCB than for parallel-beam imaging. Further, DPCB performance will be a function of radius of rotation, which will be a function of the patient's size. We believe, however, that a DPCB collimator can be designed to improve on parallel-beam collimators, even at a much larger radius.

Received Dec. 17, 2001; revision accepted Jul. 9, 2002.

For correspondence or reprints contact: David S. Lalush, PhD, Bioinformatics Research Center, Campus Box 7566, North Carolina State University, Raleigh, NC 27695-7566.

E-mail: lalush@statgen.ncsu.edu

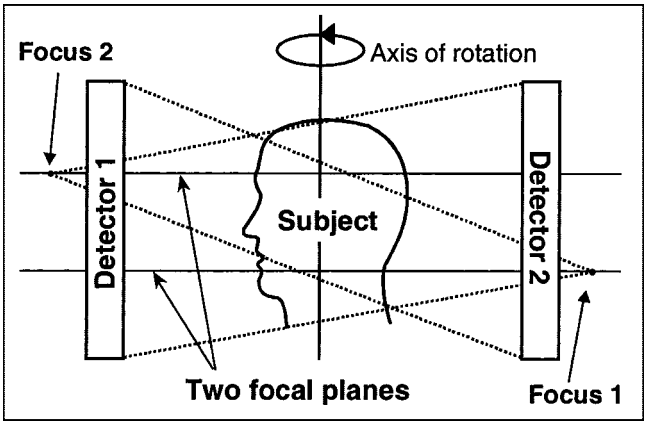

FIGURE 1. Illustration of DPCB design. Two dissimilar cone-beam collimators with focal points in different axial planes are mounted on 2 cameras of multicamera SPECT system. Gantry rotates about patient in circular orbit, as would normally occur for parallel-beam study.

In a previous study (*7*), we designed a DPCB collimator pair to be used on an ECAM dual-camera system (CTI, Knoxville, TN/Siemens Medical Systems, Inc., Hoffman Estates, IL) (Table 1), and we evaluated the design with Monte Carlo simulations to assess resolution, detection efficiency, and signal-to-noise ratios as a function of radius of rotation. In this study, we evaluated our design in the context of a task requiring human observers to find small perfusion defects in a ^{99m}Tc-hexamethylpropyleneamine oxime brain perfusion study. We had 2 working hypotheses in this study: first, that DPCB results in better detectability of small perfusion defects at all radii of rotation than does conventional parallel-beam imaging, and second, that detectability of such defects in DPCB is a function of radius of rotation. In the following sections, we detail the methods used to simulate data, perform the observer study, and analyze the outcomes.

TABLE 1
Properties of Dual-Plane Cone-Beam Collimators

Property	Value
Separation between focal planes for the 2 collimators (cm)	8
Focal length from collimator face (cm)	51.5
Hole size (hexagonal flat-to-flat) (mm)	1.5
Collimator thickness (cm)	4.5
Detection efficiency (LEHR = 1.0)	
20 cm ROR	1.50
24 cm ROR	1.93
28 cm ROR	2.47
Resolution (full width at half maximum) (cm)	
20 cm ROR	0.72
24 cm ROR	0.84
28 cm ROR	0.94
LEHR (for reference)	0.88

ROR = radius of rotation.

MATERIALS AND METHODS

Image Generation

The images used were based on the brain phantom of Zubal et al. (*8*), with uptakes and attenuation factors assigned to various regions to emulate a ^{99m}Tc-hexamethylpropyleneamine oxime brain perfusion study (Fig. 2). The Monte Carlo simulations were performed using the program SimSET (University of Washington, Seattle, WA) (*9*) to generate realistic projection data for 4 projection geometries: 3 DPCB geometries differing only in radius of rotation (20, 24, and 28 cm; 52-cm focal length) and 1 parallel geometry with a low-energy high-resolution (LEHR) collimator at a radius of rotation of 18 cm. The radii of rotation used for the DPCB geometries were determined from ergonomic statistics of humans (*10*). They corresponded to the radius required to clear the shoulders of the 5th-percentile female shoulder width (20 cm), the 50th-percentile male shoulder width (24 cm), and the 95th-percentile male shoulder width (28 cm). Thus, they provided a range of radii that encompassed most clinical cases. These radii of rotation were measured from the face of the collimator.

We simulated 7 billion photon histories per geometry to generate effectively noise-free datasets. The simulations included the effects of scatter, attenuation, and detector response. The projection datasets were taken for 128 views over a 360° rotation for each camera, on 3-mm square projection bins. The energy window was set to a typical 20% window centered at 140 keV. Further details on the simulation have been published (*7*).

We also simulated data for 4 approximately spheric defects placed at different locations in the brain. The locations were in the gray matter of the hippocampus, the postcentral gyrus, the thalamus, and the inferior temporal gyrus (Fig. 3). The defects were approximately 6–7 pixels (1.8–2.1 cm) in diameter, and their volumes ranged from 1.94 to 2.51 cm^3. To generate datasets with defects, we subtracted these defect projections from the brain projections. Scaling was adjusted so that the defect contrast (1 − defect/gray matter) in the noise-free images was 60%.

For each geometry, we generated an ensemble of 200 noisy datasets by simulating Poisson variations in each projection bin. Noise was simulated for count levels approximately 14% of those that would be expected in the clinic so that the test would be of the proper level of difficulty (*11,12*). Thus, the parallel dataset had a total of about 688,000 counts totaled between both cameras. The DPCB sets were scaled accordingly so that each configuration was simulated for the same total imaging time. The 200 noisy datasets were evenly divided between normal and defect cases. The 100 defect cases were evenly divided among the 4 defect locations. No defect image had more than 1 defect.

Each noisy projection dataset was reconstructed using 5 iterations of ordered-subset expectation maximization (*13*). Projections

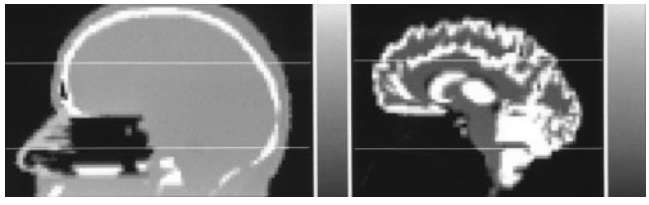

FIGURE 2. Sagittal views of brain phantom of Zubal et al. (*8*) configured as attenuation distribution (left) and emission distribution (right). Horizontal lines indicate locations of the 2 cone-beam focal planes. (Reprinted with permission of (*6*).)

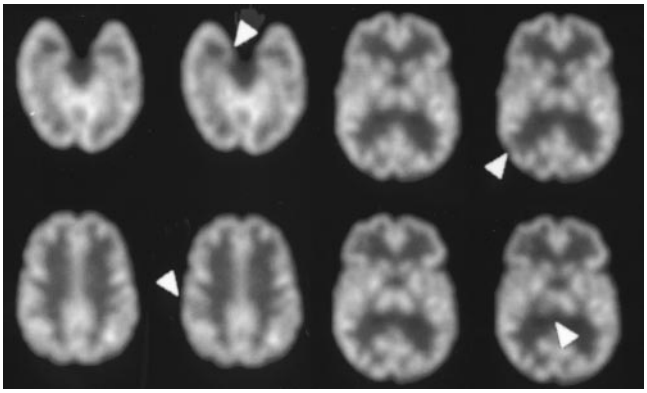

FIGURE 3. Slices from noise-free images show locations of the 4 defects (arrowheads) used in observer study. For each pair, defect-absent image is on left and defect-present image is on right. Images are noise-free reconstructions from DPCB 20 cm.

were organized with 8 subsets of 32 views each, 16 of which were obtained from each camera. Consecutive subsets were spaced as far apart as possible. The reconstruction was performed on a grid of 3-mm cubic voxels (128 × 128 per slice and 82 slices) and modeled only the effects of nonuniform attenuation. The noisy reconstructions were filtered with a 3-dimensional Butterworth filter of order 4 and cutoff 0.25 cycles per pixel. From each reconstruction, we extracted 4 slices around the location of the defect (or potential defect in the defect-free images) and assembled these 4 into a single image to be presented to the observers.

Observer Study Procedure

We recruited 8 observers from our laboratory to perform the test. These 8 were all postdoctoral trainees or graduate students with experience in SPECT imaging. None had previously worked on this project. Each observer was given instructions on the purpose of the study and was shown a demonstration comparing the defect-present and defect-absent noise-free images side by side. The observers were also instructed on the operation of the graphical user interface application for displaying and recording ratings of images.

Each observer viewed images for 2 sessions on consecutive days. Table 2 shows the organization of each session and the blocks of images in each. Session one averaged 75 min, and session 2 averaged 37 min. Each block contained images from a single configuration (LEHR, DPCB 20 cm, DPCB 24 cm, or DPCB 28 cm), but different defect locations were shown in random order within the blocks. The ordering of the blocks and the ordering of images within the blocks was randomized and different for all observers to avoid reading-order effects (*11*,*12*). Each of the 4 configurations was represented in one of the train/test sets in each session; thus, each configuration was tested on each day. Ultimately, all observers were trained using the same set of images and were tested using the same set of images, although in different order.

In training blocks, the observer was asked to view the noisy images, with the potential defect location identified by removable crosshairs. After the user chose a rating on a continuous scale from 1 to 5, the application displayed the noise-free reconstructed image with feedback on whether the defect was truly absent or present. User ratings for training sets were discarded. For testing blocks, the user was not shown the true result, and the ratings were saved.

Ratings for each of the 8 observers were compiled and analyzed using the program ROCKIT (University of Chicago, Chicago, IL) (*14*). The program estimates a binormal model to fit observer study data and computes the parameters of the associated receiver operating characteristic (ROC) curve. For each observer, we estimated an ROC curve and the area under the curve (Az) for each of the 4 imaging configurations. We also averaged the values of the fit parameters to create overall ROC curves for the observer population (*15*) and estimated the variances of those parameters to be used in significance testing.

RESULTS

Individual Observers

The estimated Az values and their SEs for each observer and each configuration are shown in Figure 4. Most, but not all, observers performed best with DPCB 20 cm and worst with LEHR. The SEs allowed us to perform significance testing for the individual observer results by comparing each pair of imaging configurations. The number of observers for whom significant differences in Az existed for each pair is shown in Table 3. Significance was set at a threshold of $P < 0.05$, or 95% confidence. For at least 3 of the 8 observers, significant differences existed for all comparisons except DPCB 20 cm to DPCB 24 cm.

Overall Results

We compiled average ROC curves for each configuration by averaging the 2 fit parameters estimated by the ROCKIT program among the different observers. These ROC curves are plotted in Figure 5, which shows a distinct rank ordering of the imaging configurations. Although this method provided a visual interpretation of the different methods' average performance, we could not assess statistical significance from the plots. Thus, we performed a paired *t* test to estimate the improvement in Az afforded by one imaging configuration over another by taking all possible pairs and computing the Az differences over the population of observers. These results are summarized in Table 4. The

TABLE 2
Organization of Observer Sessions

Session one	Session two (next day)
Large training set 1 (48 images)	Small training set 5 (24 images)
Large training set 2 (48 images)	Testing set 5 (52 images)
Large training set 3 (48 images)	
Large training set 4 (48 images)	Small training set 6 (24 images)
	Testing set 6 (52 images)
Small training set 1 (24 images)	
Testing set 1 (52 images)	Small training set 7 (24 images)
	Testing set 7 (52 images)
Small training set 2 (24 images)	
Testing set 2 (52 images)	Small training set 8 (24 images)
	Testing set 8 (52 images)
Small training set 3 (24 images)	
Testing set 3 (52 images)	
Small training set 4 (24 images)	
Testing set 4 (52 images)	

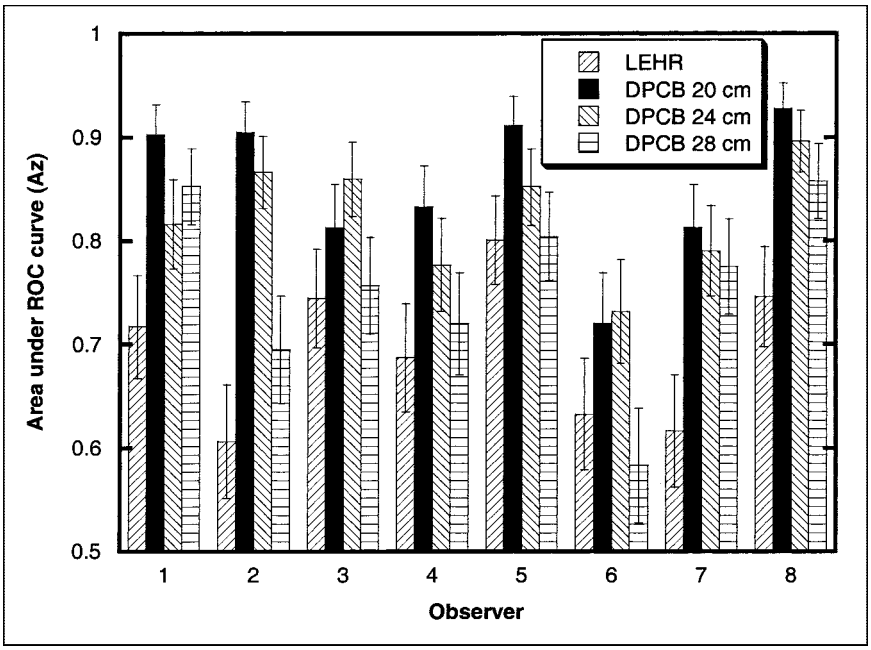

FIGURE 4. Areas under estimated ROC curves for each observer and each imaging configuration. Error bars indicate 1 SE on either side of estimate.

confidence intervals for each comparison are plotted in Figure 6. All comparisons were found to be significant at a threshold of $P < 0.05$, except DPCB 20 cm to DPCB 24 cm. The confidence interval on the improvement in Az for DPCB at 20 cm over that for DPCB at 24 cm was −0.0058 to 0.0648, indicating that if DPCB 24 cm actually resulted in higher Az, it was only marginally higher.

DISCUSSION

The results of the study were quite clear. The first hypothesis, that DPCB results in better detectability of small perfusion defects than does LEHR, was proven from the data. All 3 radii of rotation for DPCB, compared with the LEHR case, showed statistically significant improvements in Az. Although the widest radius of rotation showed the smallest improvement in Az, the confidence interval indicated that, at worst, detection performance at 28 cm was just as good as that obtained with LEHR. However, because the 28-cm radius represented the 95th percentile of male shoulder width, we would expect to have a small number of patients requiring that radius.

TABLE 3
Number of Observers with Statistically Significant ($P < 0.05$) Differences in Az for Comparisons Between the 4 Imaging Configurations

	DPCB 20 cm	DPCB 24 cm	DPCB 28 cm
DPCB 24 cm	1		
DPCB 28 cm	4	3	
LEHR	6	4	3

Total number of observers was 8.

The second hypothesis, that DPCB detectability is a function of radius of rotation, was also proven, though perhaps not as strongly. Although significant improvements in Az resulted from both DPCB 20 cm and DPCB 24 cm, compared with DPCB 28 cm, our test was not sensitive enough to determine whether the difference in performance between DPCB 20 cm and DPCB 24 cm was significant. Given the trends in Az and the conventional wisdom about SPECT imaging ("closer is better"), we conclude

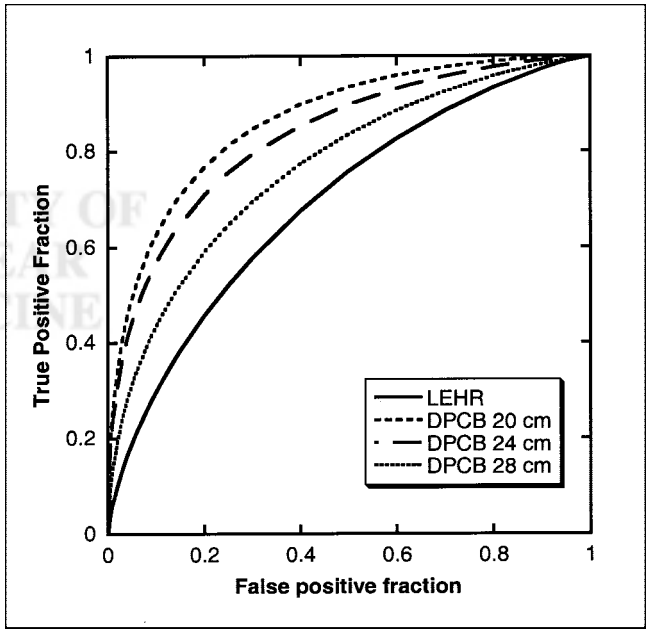

FIGURE 5. Aggregate ROC curves for each imaging configuration. These curves were computed by averaging the 2 parameters fit to ROC curves over estimated parameter values for the 8 observers.

TABLE 4
Difference in Az, SE, and *P* for Comparisons Among the 4 Imaging Configurations from Paired *t*-test for All Observers

Comparison	Difference	SE	*P*
DPCB 20 cm versus LEHR	0.1593	0.0261	0.0005
DPCB 24 cm versus LEHR	0.1298	0.0228	0.0007
DPCB 28 cm versus LEHR	0.0618	0.0257	0.0475
DPCB 20 cm versus DPCB 28 cm	0.0975	0.0202	0.0019
DPCB 24 cm versus DPCB 28 cm	0.0681	0.0244	0.0269
DPCB 20 cm versus DPCB 24 cm	0.0294	0.0149	0.0890

that DPCB 24 cm is unlikely to have a much higher Az than is DPCB 20 cm. On the basis of the confidence interval, DPCB 24 cm probably has a lower Az than does DPCB 20 cm. Further, the average ROC curves of Figure 5 suggested this trend. Thus, we conclude that it is generally best to keep the radius of rotation as close as possible in DPCB if the detection of small defects is paramount.

The question of the radius of rotation was raised by one of our earlier studies (*7*), which showed that the lower-frequency signal-to-noise ratio is significantly improved by increasing the radius of rotation whereas the higher-frequency signal-to-noise ratio is degraded. Thus, the results of defect detection will depend on the range of spatial frequencies that are important in detecting the given defect. More specifically, this relates to the size and shape of the defect and its surroundings. The results of our observer study showed that for the relatively small (~1.8 cm) defects we had chosen, the high-spatial-frequency response was most important in defect detection. With our small defects, we were challenging the resolution of the system. Had we chosen larger, lower-contrast defects, the 28-cm radius might have performed better, but that determination must be left to a future study. In any case, on the basis of the signal-to-noise ratio data and the observer study data, we expect DPCB to always outperform parallel-beam imaging.

Even though DPCB can result in some cone-beam artifacts that are due to insufficient tomographic data (*6*), it did not degrade performance significantly. Further, the use of ordered-subset expectation maximization reconstruction to assemble the data from the 2 different foci appeared to be quite efficient and effective in avoiding disturbing artifacts. However, all defects we studied were in regions viewed by both cameras, so that the effect of DPCB on a defect in the extreme high or low parts of the brain seen by only a single camera remains undetermined. Also, because our observers viewed only transverse slices of the brain, the artifacts from cone-beam insufficiency, which are primarily axially directed, may not have been apparent. To study such effects further, a more complex study with observers viewing a variety of orientations (transverse, sagittal, and coronal) would have to be designed.

All orbits were circular in this study. The DPCB and parallel-beam results could probably be improved by using elliptic orbits to contour the body better. This would give closer passes and better resolution as the cameras move across the face and the back of the head. This would also result in significant anisotropy in resolution, especially in DPCB, which may interfere with the detection task. A future study should examine the properties of elliptic orbits in DPCB.

We make no conclusions about the relative value of DPCB versus the other cone-beam brain imaging methods: tilted cone beam (*2*) and offset cone beam (*4*). Future studies should compare these methods to determine their relative advantages and disadvantages.

We have also not examined the performance of fanbeam or parallel ultra-high-resolution collimators, which are frequently used in clinical practice. Fanbeam performance is expected to share some properties of cone-beam performance in transverse directions and therefore should be an improvement on LEHR performance. However, because our test used transverse views only, it is not clear how signifi-

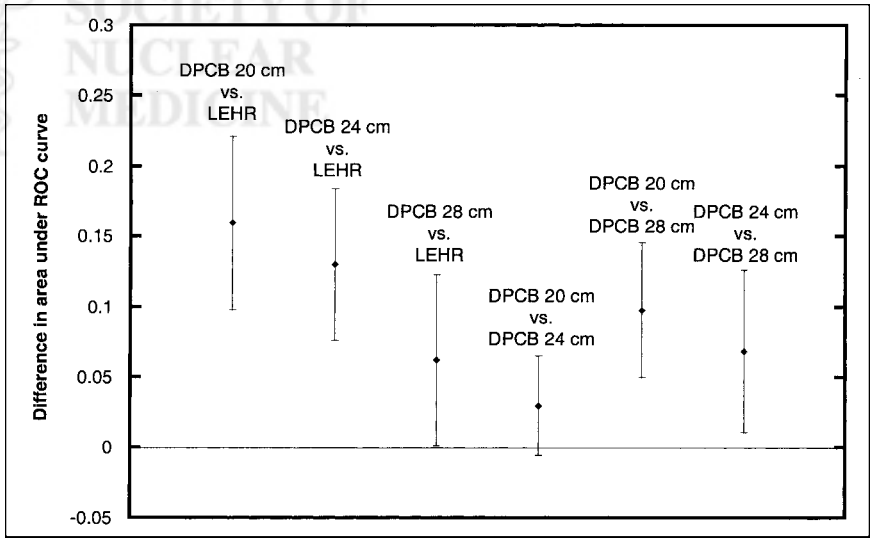

FIGURE 6. Confidence intervals at 95% on differences in Az for all possible comparisons among the 4 imaging configurations. If interval does not include zero, difference is significant at 95% confidence level.

cantly the improved axial resolution of cone-beam collimators affected the results. A future study with fanbeam collimators would help to isolate these effects.

Parallel ultra-high-resolution collimators represent a different tradeoff between noise and resolution than do LEHR collimators. The ultra-high-resolution collimator improves resolution at the expense of some detection efficiency. This effect is similar to the tradeoff we get from changing the radius of rotation in DPCB. Because we found that resolution was the most important factor for detecting small defects with DPCB, it is likely that the same situation would apply to parallel designs. Therefore, the ultra-high-resolution collimator would be expected to be somewhat of an improvement on LEHR. Another observer study would be required to quantify the improvement and also to determine just how far the efficiency/resolution tradeoff can be carried before detection performance for certain sizes and contrasts of defects is degraded.

Although observer studies must be made quite specific, we can extrapolate at least some new hypotheses to be tested from these results. First, the resolution and detection sensitivity properties of DPCB are really no different from those of a conventional cone beam with the same focal length. Thus, these results may apply in general to a conventional cone beam also. The principal difference is in the axial-direction field of view and in the fact that DPCB allows a shorter focal length for the same axial field of view. Also, there may be some differences due to the different types of incomplete-data artifacts that DPCB and a conventional cone beam would create, and the effects of these artifacts should be examined in the future with a more complex study that looks specifically at detectability in views that show axial-direction features. Further, on the basis of the geometries involved, we would expect the improvement in detectability to be a function of focal length, so that a longer-focus cone beam could still prove better than LEHR, though not much better. Finally, these results indicate that DPCB could be useful in other small-field-of-view applications, especially pediatric imaging, and future studies should also consider this possibility.

CONCLUSION

We have performed an observer study to determine the relative capabilities of dual-plane cone-beam circular-orbit SPECT in a task involving detection of small perfusion abnormalities in the brain. Our study found conclusively that dual-plane cone-beam collimators can be designed to provide better detection of such defects than can conventional LEHR parallel-beam imaging, even though a dual-plane cone beam may require much larger radii of rotation for some patients. Further, our study showed an important trend in that detectability degraded with increased radius of rotation. Thus, a dual-plane cone beam should generally be used with the smallest radius of rotation possible to maximize detection of small defects.

ACKNOWLEDGMENTS

This work was supported by a Biomedical Research Grant from the Whitaker Foundation. The authors thank the observers, Yong Du; Xin He; Stacia Sawyer; Sunita Sayeram; Paul Segars, PhD; Xi-Yun Song; Brian Yoder; and Yuchuan Wang. The authors also acknowledge the support of the staff of the Medical Imaging Research Laboratory at the University of North Carolina at Chapel Hill, whose facilities were used to perform these experiments.

REFERENCES

1. Jaszczak RJ, Floyd CE, Manglos SH, Greer KL, Coleman RE. Cone beam collimation for SPECT: analysis, simulation, and image reconstruction using filtered backprojection. *Med Phys.* 1986;13:484–489.
2. Jaszczak RJ, Greer KL, Coleman RE. SPECT using a specially-designed cone-beam collimator. *J Nucl Med.* 1988;29:1398–1405.
3. Gullberg GT, Zeng GL, Christian PE, Datz FL, Morgan HT. Cone beam tomography of the heart using SPECT. *Invest Radiol.* 1991;26:681–688.
4. Kamphuis C, Beekman FJ. A feasibility study of offset cone-beam collimators for combined emission transmission brain SPECT on a dual-head system. *IEEE Trans Nucl Sci.* 1998;45:1250–1254.
5. Lalush DS. Dual-planar circular-orbit cone-beam SPECT [abstract]. *J Nucl Med.* 1998;39(suppl):22P.
6. Lalush DS. Fourier rebinning applied to multiplanar circular-orbit cone-beam SPECT. *IEEE Trans Med Imaging.* 1999;18:1076–1084.
7. DiMeo AJ, Lalush DS. Monte Carlo simulation of dual-planar circular-orbit cone-beam SPECT [abstract]. *J Nucl Med.* 2001;42(suppl):208P.
8. Zubal IG, Harrell CR, Smith EO, Rattner Z, Gindi GR, Hoffer PB. Computerized three-dimensional segmented human anatomy. *Med Phys.* 1994;21:299–302.
9. Haynor DR, Harrison RL, Lewellen TK. The use of importance sampling techniques to improve the efficiency of photon tracking in emission tomography simulations. *Med Phys.* 1991;18:990–1001.
10. Pheasant S. *Bodyspace: Anthropometry, Ergonomics, and the Design of Work.* 2nd ed. London, U.K.: Taylor and Francis; 1998:174–178.
11. Metz CE. ROC methodology in radiologic imaging. *Invest Radiol.* 1986;21:720–733.
12. Metz CE. Some practical issues of experimental design and data analysis in radiological ROC studies. *Invest Radiol.* 1989;24:234–245.
13. Hudson HM, Larkin RS. Accelerated image reconstruction using ordered subsets of projection data. *IEEE Trans Med Imaging.* 1994;13:601–609.
14. Metz CE. *ROCKIT.* 0.9B ed. Chicago, IL: Department of Radiology, University of Chicago; 1998.
15. LaCroix KJ, Tsui BMW, Frey EC, Jaszczak RJ. Receiver operating characteristic evaluation of iterative reconstruction with attenuation correction in ^{99m}Tc-sestamibi myocardial SPECT images. *J Nucl Med.* 2000;41:502–513.